# Nonlinear dynamics optically induced in nematic liquid crystals

G. Russo, V. Carbone, and G. Cipparrone*
*Dipartimento di Fisica and Istituto Nazionale per la Fisica della Materia, Università della Calabria, 87036 Rende (CS), Italy*
(Received 21 March 2000)

We report the analysis of the dynamical regimes induced in a homeotropically aligned nematic liquid-crystal layer when an *s*-polarized laser beam impinges at a small incident angle. These regimes are studied by analyzing the time series of the variation of the polarization state of a light probe beam, recorded at different light intensities. A detailed description of the dynamical regimes, based on the analysis of the wavelet transforms performed on the observed time series, is presented. We recognize a first Hopf bifurcation followed by a gluing bifurcation, and a further transition toward an irregular regime. Similarities between our experimental results and a scenario of transition to chaos via a sequence of gluing bifurcations have been discussed.

PACS number(s): 61.30.−v, 05.45.−a, 42.65.−k

## INTRODUCTION

The dynamics of nonlinear interactions between a nematic liquid crystal (NLC) and an intense optical field has been extensively studied in the past year [1], even if for some experimental geometry a deep understanding of the phenomena needs some more careful analysis. In particular a very interesting and rich dynamics can be observed in the case of an ordinary wave that impinges with a small angle on a homeotropically aligned nematic liquid-crystal film [2]. For this experimental geometry, there are evidences of persistent stochastic oscillations of the diffraction rings, observed in the far field pattern of the transmitted beam. This phenomenon is very interesting and very easy to be reproduced, being only the result of the nonlinear coupling between the NLC birefringence and the intense optical field. The phenomenon is then described by the ''nematodynamics'' equations, coupled with the Maxwell equations describing the optical field. There are then some difficulties to solve this highly nonlinear system of equations, and models are needed. A model of this kind has been proposed by Demeter and Kramer [3], whose simulations show a transition to chaos via a sequence of successive gluing bifurcations.

In a recent paper [4], we built up an experimental tool that allows us to investigate the light transmitted by a NLC film during the induced molecular reorientation. In our experiment, a pump-probe technique and a four-detector polarimeter (FDP) allowed us to measure, with a good spatial and temporal resolution, the time evolution of the polarization state of the probe beam. The measurements show a sequence of very interesting dynamical regimes in the polarization state. In fact, as the pump beam intensity is increased, the time evolution of the polarization state evolves from a periodic regime toward a stochastic one through a series of bifurcations. The preliminary analyses reported in [4], suggest that the system exhibits a transition to chaos as the control parameter (the light intensity) increases. However, if deterministic chaos would occur in our experiments, the system would follow a very unusual route toward that chaotic regime. For this reason, we think that the observed phenomenon requires a more detailed study since it is interesting not only from the point of view of nonlinear optics of liquid crystals, but also from that of basic theory of chaos. To this aim, in the present paper, we will report a detailed analysis of the observed regimes, performed through the wavelet transforms of time series, and other usual tools of nonlinear analysis.

## EXPERIMENT

Using the experimental setup described in [4], we performed the reported measurements. The sample was a 75-$\mu$m NLC (*E*7 by Merck) cell. A probe beam (He-Ne laser), is sent at normal incidence on the NLC film and focused on the sample by a focal length shorter than that of the pump beam ($Ar^+$ laser) in order to investigate a small region in which the molecular dynamic is induced. The polarization of the transmitted probe beam is analyzed by a four-detector polarimeter (FDP), which allows us to measure the Stokes parameters. The FDP has been extensively described in [4]. From the acquired time series of the measured Stokes parameters $S_0, S_1, S_2, S_3$ we calculate [5] the azimuthal angle of the major axis $\Theta$ and the ellipticity *e*:

$$\Theta = \frac{1}{2}\arctan\left(\frac{S_2}{S_1}\right)$$

$$e = \tan\left\{\frac{1}{2}\arcsin\left[\frac{S_3}{(S_1^2+S_2^2+S_3^2)^{1/2}}\right]\right\}.$$

The measurements were performed at fixed incidence angle of about 5°. The external control parameter is $\rho = I/I_{th}$, where *I* is the pump beam light intensity and $I_{th}$ is the optical Freédericksz transition (OFT) threshold for normal incidence.

For a good identification of the different dynamical regimes induced in the system, the incident laser power is increased by small steps of the order of 6 mW, which corresponds to $\rho \approx 0.08$. Among all measurements we performed, we show here those corresponding to bifurcations representative of the different dynamical regimes.

*Corresponding author.

 

## ANALYSIS OF THE DYNAMICS

### Mathematical tools

As described in [4], the observed time series have approximately the same behavior for both $e$ and $\Theta$. Therefore we choose to report the analysis of the encountered regimes only for the ellipticity $e$ [see Figs. 1(a), 4(a), 7(a), 10(a), and 12(a)].

To search for characteristic frequencies, we use the wavelet transforms, which are mathematical tools that can unfold time series into time and frequency [6]. The wavelet transform $W(a,t)$ of a signal $f(t)$ is defined as [6]

$$W(a,t)=\int w_a(t-\tau)f(\tau)d\tau,$$

where the function $w_a(t)$ is the analyzing wavelet. The functions $w_a(t)$ are localized in time and frequency and the decomposition is obtained by dilating or contracting the wavelet before convoluting it with the signal. In this paper, we use the Morelet wavelet, defined through

$$w_a(t)=\sqrt{a}\exp\left[2\pi i\frac{t}{a}-\frac{1}{2}\left(\frac{t}{a}\right)^2\right].$$

The wavelet acts as a filter, that is, $w_a(t)$ selects the components of $f(t)$ that correspond to the frequencies in the range of amplitude $\Delta f\approx 1/a$, and centered in $f=2\pi/a$. Then the coefficient $W(a,t)$ assumes an high value when there is a contribution of the signal at the frequency $f$ and at time $t$.

The advantage with respect to the usual Fourier transforms lies in the fact that the formers, describing local properties of the signal, allows us to detect short-living structures, while with the latter one obtains only global information. We report also a two-dimensional representation of the attractors of the time series $e(t)$ (see Figs. 3, 6, 8, 11, and 13) for better information about the dynamics in the phase space. The attractors are reconstructed using the Takens method [7] that is based on the construction of a vector $\vec{x}(t)$ in the embedding phase space

$$\vec{x}(t)=[e(t),e(t+\tau),e(t+2\tau),\ldots,e(t+(d_E-1)\tau)]$$

in which $\tau$ is an appropriate time delay and $d_E$ is the embedding dimension. Usually $\tau$ is the time that corresponds to the first zero of the autocorrelation function.

### Experimental results

First of all, if $\rho<1.0$ we did not observe any variation of the probe-beam polarization state, with respect to the case of undisturbed nematic sample. That is, when $\rho<1.0$, no director distortion was induced. In the range $1.0<\rho<1.6$, the polarization state reaches a stable state when the pump beam is switched on. This state is different when compared to the undisturbed sample. This is a stable stationary state, indicating that the molecular director reaches a distorted steady state. A fixed point in the phase space represents this situation. After this state, the system bifurcates toward a new state where a periodic oscillation appears. In fact, for $1.6<\rho<1.9$, the variation in time of the polarization state shows a regular oscillating pattern around negative values of $e$ [see Fig. 1(a)].

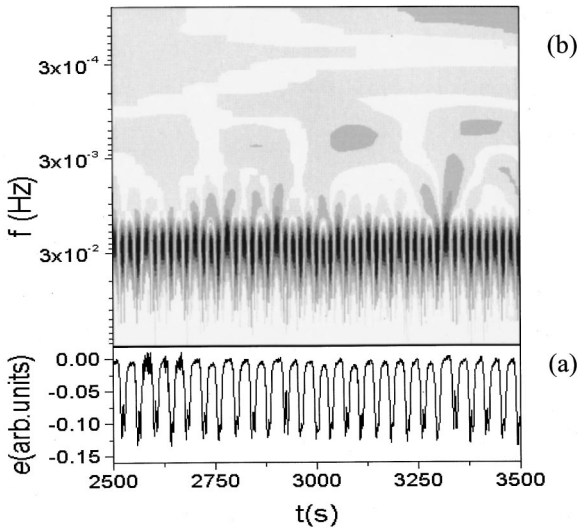


FIG. 1. We report the time series $e(t)$ (a) and the contour map of normalized wavelet coefficients $\hat{w}(a,t)=w(a,t)/|w(a,t)|_{\max}$ in the time-frequency plane (b) for $\rho=1.8$. Dark regions correspond to values $|\hat{w}(a,t)|=1$, white regions correspond to $|\hat{w}(a,t)|=0$. We used 15 steps between these extreme values.

Looking at the normalized wavelet coefficients $\hat{w}(a,t)=w(a,t)/w(a,t)_{\max}$ [Fig. 1(b)], we can recognize some characteristic frequencies. This is a well-defined periodic regime even if the oscillations appear to be not sinusoidal. The signal is made by two main frequencies characterized by the highest absolute values of the wavelets coefficients. In Fig. 2, we report the time evolution of the wavelet coefficient $\hat{w}(a,t)$ for both frequencies $f_0=26$ mHz and $f_1=52$ mHz. As shown in Fig. 2, the signal can then be described by a

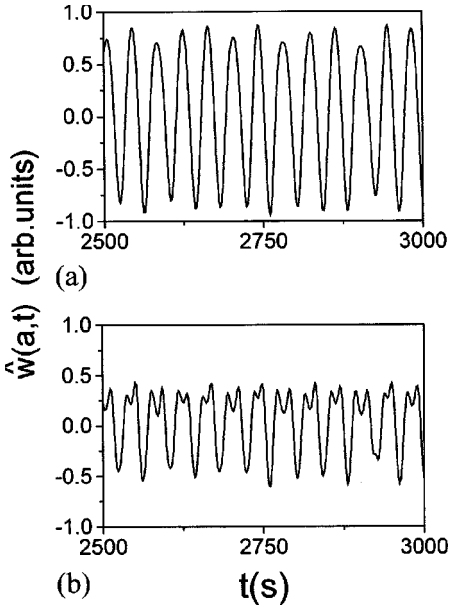


FIG. 2. We report the time evolution of wavelet coefficients $\hat{w}(a,t)$ for two different frequencies, namely, $f_0=26$ mHz (a) and $f_1=52$ mHz (b). These frequencies correspond to the highest absolute values of wavelet coefficients for $\rho=1.8$.

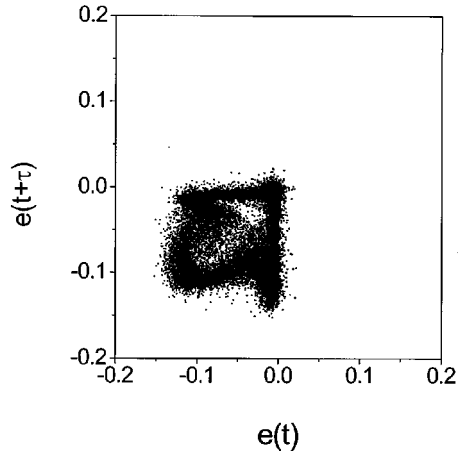


FIG. 3. The reconstructed attractor in the phase space for $\rho = 1.8$, that is, $e(t+\tau)$ vs $e(t)$ for $\tau = 9$ s.

sum of two main modes: a periodic function [Fig. 2(a)] and periodic pulses [Fig. 2(b)].

In the phase space, the transition from the distorted steady state to regular oscillations corresponds to an Hopf bifurcation and the attractor of the time series becomes a limit cycle (Fig. 3) as on attends for a periodic regime. In the range $1.9 < \rho < 2$, we observe a regime characterized by time intervals during which the oscillations are centered on both positive and negative values of $e$ [see Fig. 4(a)]. During this regime it is possible to observe two equilibrium states characterized by a left elliptical polarization and a right elliptical polarization. These states are unstable in the sense that the system oscillates between both states, and the changes happen at random times. This is of course a new periodic regime, but looking at the wavelet coefficients [Fig. 4(b)] we can observe the birth of very intense low-frequency components while the high frequencies components are now weak. Nevertheless the wavelet transform emphasizes few interesting characteristics. As shown in Fig. 4(b), the signal is totally driven by the low-frequency components. In fact, when a change in the sign of the ellipticity $e(t)$ occurs, we observe a spike that involves a wide range of frequencies, from lower

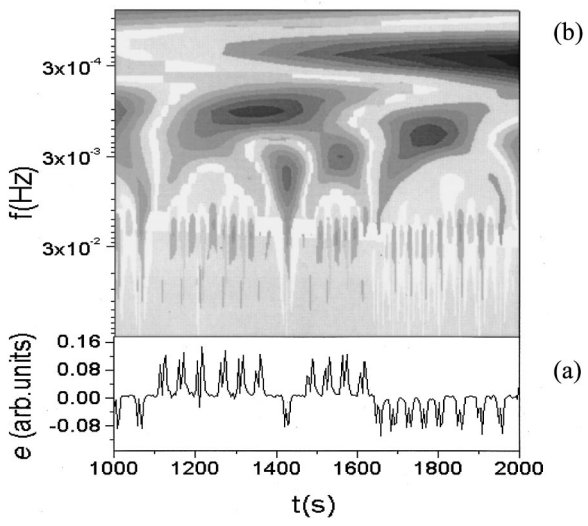


FIG. 4. The same as Fig. 1 for $\rho = 1.9$.

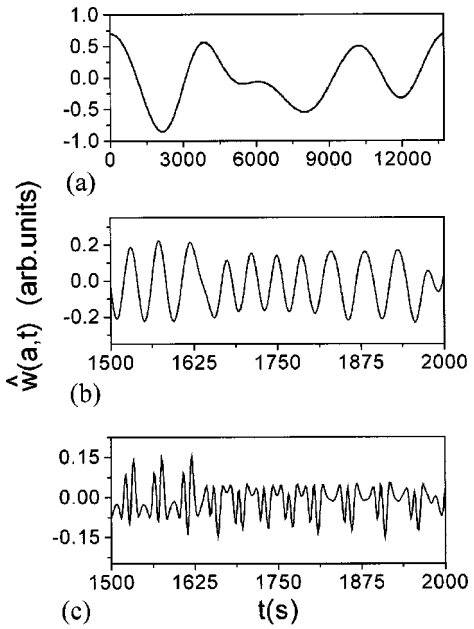


FIG. 5. We report the time evolution of wavelet coefficients $\hat{w}(a,t)$ for three different frequencies, namely, $f_0 = 0.25$ mHz (a), $f_1 = 21$ mHz (b), and $f_2 = 63$ mHz (c). These frequencies correspond to the highest absolute values of wavelet coefficients for $\rho = 1.9$.

to higher. This suggests that a low-frequency modulation is the source of the switching between the two polarization stable states. In Fig. 5 we report the time evolution of the three characteristic frequencies with the higher absolute value of the wavelet coefficients, namely, $f_0 = 0.25$ mHz, $f_1 = 21$ mHz, and $f_2 = 63$ mHz, respectively. As it can be seen the signal can be still represented as a sum of a periodic function [Fig. 5(a)], periodic pulses [Fig. 5(b)], and a nonperiodic low-frequency contribution [Fig. 5(c)]. However, in this case the low-frequency modulation is the nonperiodic dominant contribution, and this determines the switching between positive and negative values.

The attractor in the phase space is made by two cycles (Fig. 6) in which the phase trajectories are confined for a given time. This time corresponds to the duration of the interval in which oscillations are either positive or negative. When $e(t)$ changes sign, the system jumps on the other

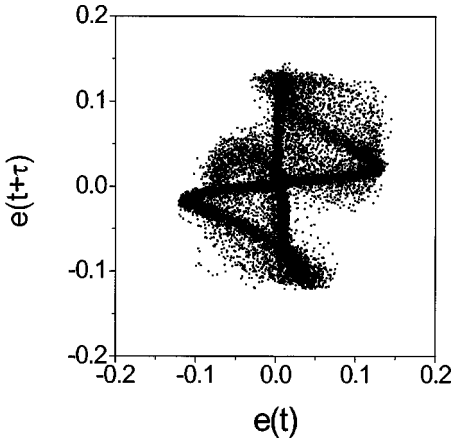


FIG. 6. The reconstructed attractor in the phase space for $\rho = 1.9$, that is, $e(t+\tau)$ vs $e(t)$ for $\tau = 100$ s.

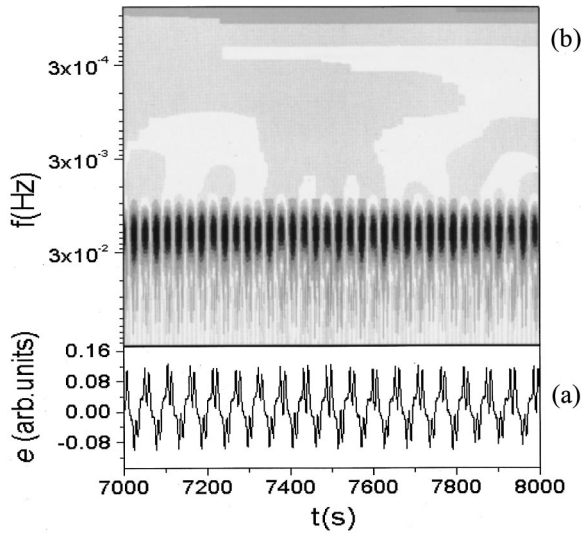


FIG. 7. The same as Fig. 1 for $\rho=2.3$.

cycle, where it remains for a given time (in general different from the previous one). As a characteristic feature, we observed that the average time intervals during which the system is confined to a single polarization state tends to decrease as $\rho$ increases. This behavior suggests that we are observing a transition toward a new regime characterized by regular oscillations between the two polarization states above mentioned. This new regime, shown in Fig. 7(a), is observed in the range $2<\rho<2.6$. The transition between the periodic regime at $\rho\leqslant 1.9$, and the new periodic regime which we observe when $\rho\geqslant 2$, is due to a different kind of bifurcation, because both periodic regimes are not exactly the same in the phase space. We will discuss this later. Looking at the wavelet coefficients map [Fig. 7(b)], we can recognize that the transition represents a kind of ''self-organization'' of the signals. In fact, the measured quantity is periodic for $\rho=1.8$, looks to be ''quasistochastic'' for $\rho=1.9$ (in the sense that some low frequencies are visible), but is again periodic for $\rho=2.3$. All frequencies, which were visible in Fig. 4(b), are completely suppressed for $\rho=2.3$, and the coefficients map [Fig. 7(b)] is very similar to those of the first periodic dynamical regime [Fig. 1(b)]. Nevertheless, a difference between this new regime and the case at $\rho=1.8$, is the birth of an intense activity at higher frequencies, as shown in Fig. 7(b). In the phase space, the two previous cycles are now merged forming a single limit cycle (Fig. 8) more structured and covering a range in the phase space that is wider than that shown in Fig. 3 for $\rho=1.8$. This regular regime [Fig. 7(a)] can be observed up to the value $\rho=2.6$. Even in this case, we can build up the signal with a periodic function ($f_0=18$ mHz) [Fig. 9(a)] and a function made by some periodic pulses with stochastic amplitudes [Fig. 9(b)].

As shown in Fig. 10(a) in the range $2.6<\rho<3.0$, we observe a new irregular sequence of time oscillations, which looks to be similar to that observed for $1.9<\rho<2$. Even in this case, the wavelet coefficients map [see Fig. 10(b)] shows the presence of intense low-frequency structures, which determines the modulation in the amplitude of the signal. Nevertheless in this case the switching between intervals in which the system reaches a single polarization state is less pronounced.

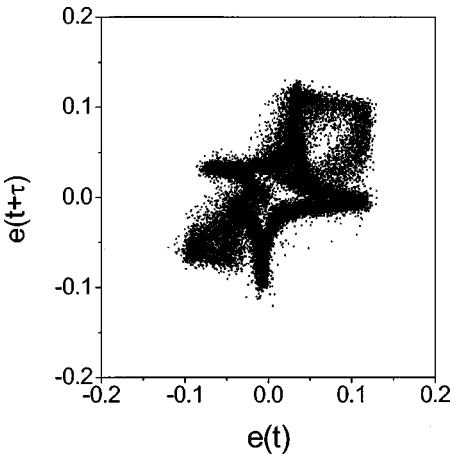


FIG. 8. The reconstructed attractor in the phase space for $\rho=2.3$, that is, $e(t+\tau)$ vs $e(t)$ for $\tau=9$ s.

The attractor shows a gradual disruption of the regular structures observed in the previous regimes, and it covers a larger area in the phase space (see Fig. 11). This regime represents the transition to a stochastic dynamical behavior that occurs for higher values $\rho>3.0$ [Fig. 12(a)].

In the wavelet coefficient map [see Fig. 12(b)] as the stochastic regime appears, we can observe a continuous-frequency spectrum and an irregular splitting of frequencies, from lower to higher. In this regime, a disordered set of point constitutes the attractor in the phase space (Fig. 13).

The measurements we described show the evidence of a rich dynamical behavior that requires a more detailed investigation, mainly as concern the physical description of the sequence of bifurcations which, to our knowledge, are never observed up to now. In fact, the results of our preliminary analysis, that is the wavelet transforms and the reconstruction of the phase space, suggest the presence of a transition to a chaotic behavior in the measured quantities, as the control parameter increases.

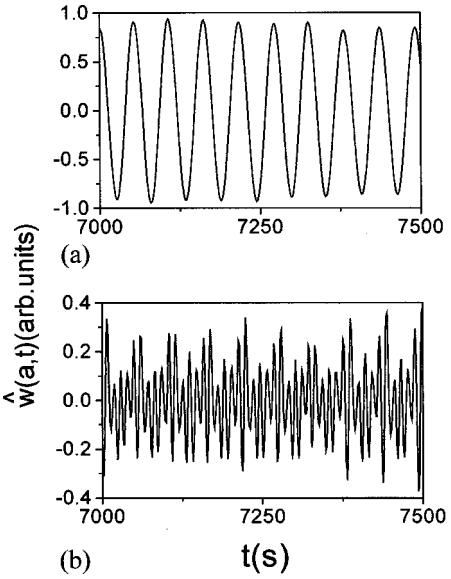


FIG. 9. We report the time evolution of wavelet coefficients $\hat{w}(a,t)$ for three different frequencies, namely, $f_0=18$ mHz (a), $f_1=85$ mHz (b). These frequencies correspond to the highest absolute values of wavelet coefficients for $\rho=2.3$.

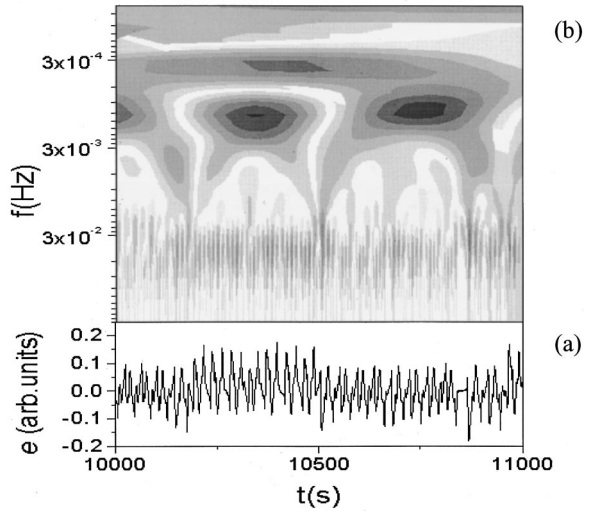


FIG. 10. The same as Fig. 1 for $\rho=2.8$.

In a recent paper [3], Demeter and Kramer proposed a model for the director dynamics induced in our experimental geometry. Using the equations describing the coupling between a nematic liquid crystal and an optical field, they obtained a set of truncated nonlinear differential equations. Simulations of the equations so obtained show that as the intensity field is increased, the system reaches a chaotic state through an unusual route to chaos via an infinite sequence of ''gluing'' bifurcations. According to the scenario proposed in that paper [3], as the light intensity exceeds the OFT threshold, a stationary reoriented state occurs. Further enhancement of the control parameter induce a Hopf bifurcation and two simple limit cycles appear in the phase space, which are mutual images under the transformation that keeps account of the liquid crystal (LC) molecules inversion symmetry. As the light intensity is increased, the two limit cycles merge in a gluing bifurcation at the origin that represents a saddle point. Increasing the control parameter, the two limit cycles split and two new asymmetric limit cycles appear. The sequence of splitting and remerging of the limit cycles continues until the control parameter reaches a limit value after which the motion becomes chaotic.

Looking at our experiment, we can observe very interesting analogies with the picture proposed by Demeter and

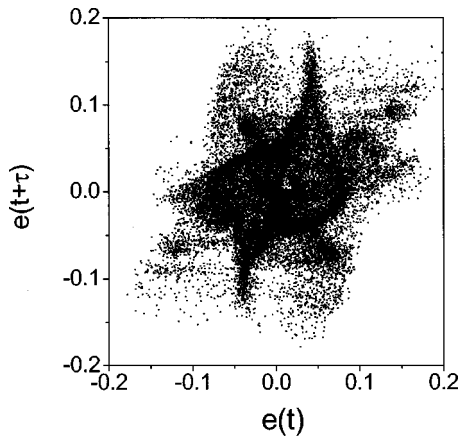


FIG. 11. The reconstructed attractor in the phase space for $\rho=2.8$, that is $e(t+\tau)$ vs $e(t)$ for $\tau=5$ s.

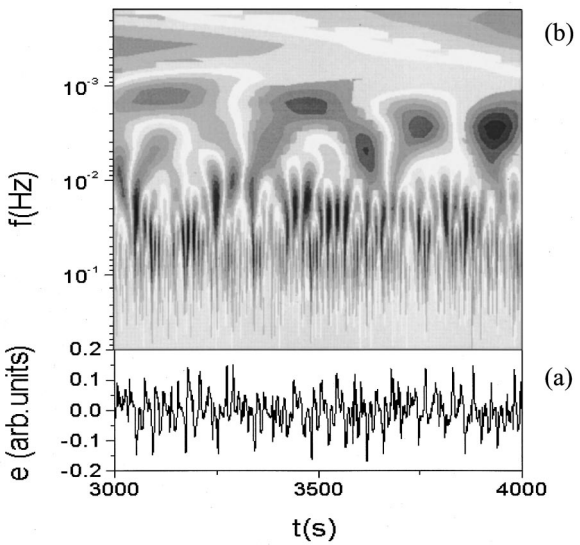


FIG. 12. The same as Fig. 1 for $\rho=4.1$.

Kramer [3]. In fact as the control parameter is increased, our measured quantities, that are related to the orientation of the molecular director [8], show a stationary reoriented state, followed by an Hopf bifurcation. The successive regime ($1.9<\rho<2$) could be interpreted as driven by a gluing bifurcation. In fact, the phase space is made by two limit cycles that merge at the origin. In fact, every time the measured quantity switches from positive to negative values, or vice versa [Fig. 4(a)], the point representing the system state in the phase space, jumps from a limit cycle to the other one (Fig. 6). Note that, when the system lies near the origin, the experimental noise acts as a weak perturbation and this determines what is the limit cycle in which the phase trajectories will be confined for a given time interval.

After this bifurcation ($2<\rho<2.6$), we observe a reorganization of the signal and a fusion of the two-limit cycle forming another one more complex, which can be interpreted as the periodic regime after the first theoretic gluing bifurcation. However, as the intensity is increased, we do not observe further gluing bifurcations, but we observe a transition toward an irregular stochastic regime.

To investigate this last regime, we use the usual tools for the reconstruction of the dynamical properties of a measured

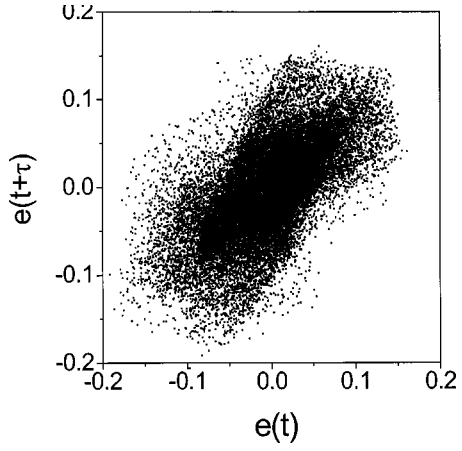


FIG. 13. The reconstructed attractor in the phase space for $\rho=4.1$, that is, $e(t+\tau)$ vs $e(t)$ for $\tau=2$ s.

chaotic time series that consists of two steps: the determination of the largest Lyapunov exponent of the trajectories embedded in the phase space and the fractal dimension of the attractor. We calculated the Lyapunov exponent λ of the time series $e(t)$ using the Wolf method [9]. This method allows us to calculate the average rate of the divergence of the trajectories on the attractor in the embedding phase space. Using time series measurements in the regular regimes ($1.6<\rho<3.0$) the Lyapunov exponent seems to converge toward the value $\lambda \approx 10^{-5}\,\mathrm{s}^{-1}$, close to zero as we expect for a periodic signal, whereas for measurements in the irregular regimes ($\rho>3.0$) we found a convergence toward $\lambda \approx 10^{-3}\,\mathrm{s}^{-1}$. The last value of λ does not suffice to establish whether either deterministic chaos or a stochastic random phenomenon drives the dynamic of the polarization state for higher values of the intensity. In fact, two fundamental problems, depending on the experimental conditions, occur in the determination of the Lyapunov exponent. (1) The experimental noise could mask the real nature of the attractor; (2) the finite length of the time series is not long enough to realize a correct analysis. In fact, a limited time series in a system with a slow dynamics, does not provide a sufficient number of trajectories on the attractors for a correct estimate of the Lyapunov exponent. Unfortunately, the measurements of longer time series are prevented by experimental limitations. In fact when the irregular regimes occurred, we observed that the molecular anchoring is broken after a few hours. This phenomenon can be attributed to the dynamics induced in the system in our geometry. In fact, we repeated the experiments with the same high intensity values $\rho$ by using normal incidence of the laser beam. In this geometry, we observe a distorted stable stationary state of the molecular director [1]. We found that the molecular anchoring persists for a longer period with respect to the period of our time series.

To make an estimate of fractal dimension of the irregular attractor ($\rho>3.0$) we have used the well-known method proposed by Grassberger and Procaccia [10] that consists of the calculation of the correlation dimension $\nu$ by means the correlation sum $C(r)$ defined by

$$C(r) = \frac{1}{N^2}\left\{\begin{array}{l}\text{the number of pairs } \vec{r}(t_i) \text{ and } \vec{r}(t_j) \text{ such that}\\ \text{the distance among the pair is less than } r\end{array}\right\}$$

$$= \frac{1}{N^2}\sum_{i,j=1}^{N} H(r-|\vec{r}_i-\vec{r}_j|),$$

in which $N$ is the total number of points on the attractor and H is the Heaviside function.

As Grassberger and Procaccia showed, the correlation dimension $\nu$ of the attractor can be found from the scaling relation $C(r)\approx r^{\nu}$. If the embedding dimension $d_{\mathrm{E}}$ is large enough (in general it suffices that $d_E>2\nu+1$), the slope of the plot settles down to a value that does not depend on $d_{\mathrm{E}}$. In Fig. 14(a), the curves $\log_{10}[C(r)]$ vs $\log_{10}(r)$ are plotted for different values of $d_{\mathrm{E}}$. Then we calculated the value of $\nu$ by a least-squares fit in the linear range of the plots, and the values of $\nu$ as a function of the embedding dimensions are reported in Fig. 14(b). As it can be seen, the values of the dimension continue to increase, so that we cannot affirm that the attractor in the phase space has a typical dimension. Even in this case, experimental problems do not allow us to determine whether chaos occurs in our experiment or a stochastic regime is reached.

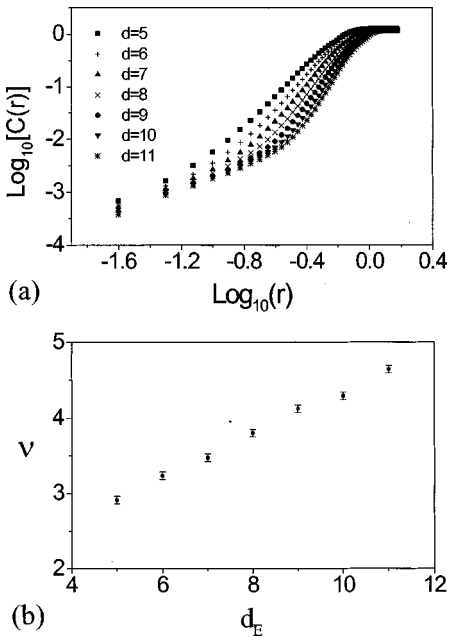


FIG. 14. (a) $\log_{10}[C(r)]$ vs $\log_{10}(r)$ for different values of the embedding dimension $d_{\mathrm{E}}$; (b) correlation dimension $\nu$ vs $d_{\mathrm{E}}$.

## DISCUSSIONS AND CONCLUSIONS

In the present paper, we reported the analysis of the dynamical regimes optically induced in an NLC film as the intensity of a laser beam increases. We use an experimental setup based on a pump-probe technique and a four-detector-polarimeter. This apparatus allows us to get information with a very good temporal end spatial resolution on the variation in the polarization state of the probe laser beam by measuring the time evolution of the Stokes parameters. Measurements show a rich variety of dynamical regimes as the pump intensity increases. The sequence of bifurcations we observe is very interesting and deserves further studies. The analysis of the observed time series at different intensities suggests the presence of a transition toward a chaotic regime in the system. Unfortunately, an estimate of the maximum Lyapunov exponent does not allow us to confirm whether or not deterministic chaos is present. This is due to severe experimental limitations, that is a slow dynamics with some noise and a limited possibility to get longer time series, due to the breaking of the molecular anchoring.

As a comparison, we recover very surprising qualitative analogies between our experimental results and the scenario proposed by Demeter and Kramer [3]. In particular, we found good agreement at least for small intensity values. Perhaps this is due to the fact that the approximations in Ref. [3] are consistent only for small $\rho$. We think that the model proposed by Demeter and Kramer [3] is able to predict the first Hopf bifurcation and the subsequent gluing bifurcation. For large values of $\rho$, that is when several diffraction rings are visible, the small angle approximation used in the model

[3] is no longer satisfied. Moreover, the sequence of bifurcations values for the intensity parameter, predicted for the gluing sequence, accumulates in a very small range that depends on the incidence angle. On the other hand, experimental results cannot give a clear indication whether further gluing bifurcations and chaos is present in the experiment. Further experimental results are underway with different incidence angles, in order to achieve a finer scanning with longer time series.

**ACKNOWLEDGMENTS**

The authors are grateful to Dr. C. Versace and Dr. G. Strangi for the building of the four-detector polarimeter. We are also grateful to professor P. Palffy-Muhoray for useful discussions and to Dr. Gabor Demeter for sending us his papers prior to publication.

[1] N. V. Tabiryan, A. V. Sukhov, and B. Y. Zel'dovich, Mol. Cryst. Liq. Cryst. **136**, 1 (1986).

[2] G. Cipparrone, V. Carbone, C. Versace, C. Umeton, R. Bartolino, and F. Simoni, Phys. Rev. E **47**, 3741 (1993); V. Carbone, G. Cipparrone, C. Versace, C. Umeton, and R. Bartolino, *ibid.* **54**, 6948 (1996); E. Santamato, P. Maddalena, L. Marrucci, and B. Piccirillo, Liq. Cryst. **25**, 357 (1998), and references therein.

[3] G. Demeter and L. Kramer, Phys. Rev. Lett. **83**, 4744 (1999).

[4] G. Cipparrone, G. Russo, C. Versace, G. Strangi, and V. Carbone, Opt. Commun. **173**, 1 (2000).

[5] R. M. A. Azzam and N. M. Bashara, *Ellipsometry and Polarized Light* (North-Holland, Amsterdam, 1977).

[6] M. Farge, Annu. Rev. Fluid Mech. **24**, 395 (1992).

[7] F. Takens, *Dynamical Systems and Turbulence, Warwick*, Lecture Notes in Mathematics Vol. 898 (Springer, Berlin, 1980), p. 366.

[8] D. W. Berreman, J. Opt. Soc. Am. **62**, 502 (1972); P. Allia, M. Arlone, C. Oldano, and L. Trossi, Mol. Cryst. Liq. Cryst. **179**, 253 (1990); K. Eidner, G. Mayer, M. Schmidt, and H. Schmiedel, *ibid.* **172**, 191 (1989).

[9] A. Wolf, J. B. Swift, H. L. Swinnwy, and J. A. Vastano, Physica D **16**, 285 (1985).

[10] P. Grassberger and I. Procaccia, Phys. Rev. Lett. **50**, 346 (1983).